HHS Public Access

A dextran-based probe for the targeted magnetic resonance imaging of tumours expressing prostate-specific membrane antigen

Guanshu Liu[1,2,*], **Sangeeta Ray Banerjee**[1], **Xing Yang**[3], **Nirbhay Yadav**[1,2], **Ala Lisok**[1], **Anna Jablonska**[1], **Jiadi Xu**[1,2], **Yuguo Li**[1,2], **Martin G. Pomper**[1], and **Peter van Zijl**[1,2,*]

[1]The Russell H. Morgan Department of Radiology and Radiological Science, Johns Hopkins School of Medicine, Baltimore, MD, USA

[2]F.M. Kirby Research Center for Functional Brain Imaging, Kennedy Krieger Institute, Baltimore, MD, USA

[3]Department of Nuclear Medicine, Peking University First Hospital, Beijing, China

Abstract

Safe imaging agents able to render the expression and distribution of cancer receptors, enzymes or other biomarkers would facilitate clinical screening of the disease. Here, we show that diamagnetic dextran particles coordinated to a urea-based targeting ligand for prostate-specific membrane antigen (PSMA) enable targeted magnetic resonance imaging (MRI) of the PSMA receptor. In a xenograft model of prostate cancer, micromolar concentrations of the dextran –ligand probe provided sufficient signal to specifically detect PSMA-expressing tumours via chemical exchange saturation transfer MRI. The dextran-based probe could be detected via the contrast originating from dextran hydroxyl protons, thereby avoiding the need of chemical substitution for radioactive or metallic labelling. Because dextrans are currently used clinically, dextran-based contrast agents may help extend receptor-targeted imaging to clinical MRI.

Receptor-targeted clinical imaging is currently only performed using radionuclide-based techniques such as positron emission tomography (PET)[1]. MRI using paramagnetic labels has shown potential for receptor imaging of, for example, folic acid[2], transferrin[3], HER-2/neu[4] and, recently, prostate-specific membrane antigen (PSMA)[5–7]. However, the clinical translation of these probes has proved elusive. Instead, a non-metallic, non-radioactive and biodegradable particle conjugated with a low-molecular-weight affinity

Correspondence to Guanshu Liu, Ph.D. guanshu@mri.jhu.edu, and Peter van Zijl, Ph.D. pvanzijl@jhu.edu.

agent is less likely to elicit an immune response than, for instance, an anti-PSMA antibody[8]. These constrains should provide a stimulus for nanotechnology approaches to become more commonly used in clinical settings. Here we report the design of a biodegradable MRI agent based on dextran (a nanoscale branched macromolecule) conjugated with a low-molecular-weight, urea-based ligand (Fig. 1a) for targeting and imaging PSMA, an enzyme that is overexpressed on prostate cancer cells and within the tumour neovasculature, and whose expression in limited to only a few normal tissues. Instead of using chemical or metallic labelling, we applied radio-frequency (RF)-based magnetic labelling of dextran hydroxyl protons (Fig. 1b, also see Supplementary Fig. S1 for molecular weight-dependent and Fig S2. for saturation parameters-dependent CEST signal of dextrans), which can be achieved non-invasively *in situ*. As magnetic labelling, we used RF saturation, which was subsequently transferred to the water using chemical exchange saturation transfer (CEST; a sensitivity-enhancement approach) MRI (Fig. 1c)[9–12]. CEST–MRI enabled the detection of micromolar concentrations of 10 kD dextran–urea constructs in vivo by imaging changes in the water signal (changes in proton concentration of about 1.1 M).

Results

To achieve a low background signal and an increase target-to-background ratio, we chose 10 kD dextran (Dex10), which has a hydrodynamic diameter of 4–6 nm (ref. [13]) and can easily penetrate tumours but is quickly washed out from the extracellular space within half an hour[14]. In comparison, dextran of higher molecular weights (MWs) would accumulate for much longer time in the extravascular space of the tumours, making it difficult to detect specific binding. We synthesized PSMA-targeted CEST MRI agents by conjugating Dex10 with a low-molecular-weight, urea-based PSMA targeting ligand (MW ~ 400) according to the scheme in Fig. 2a. The binding affinity to PSMA (PSMA inhibitory activity) of the conjugated materials was measured using a standard fluorescence-based assay that tests the inhibitory ability of a compound with respect to hydrolysis of N-acetylaspartylglutamate (NAAG) into glutamate for the lysates of PSMA-positive human prostate adenocarcinoma (LNCaP) cells[6,15]. Compared with the non-conjugated amino-Dex10 (compound **1**; Fig. 2a), which showed no binding affinity ($K_i > 1$ μM) to PSMA, the conjugated material urea–Dex10 (compound **3**; Fig. 2a) exhibited a much higher binding affinity, with a $K_i = 2$ nM ($IC_{50} = 10$ nM; Fig. 2b).

Figures 3a,b compare the CEST–MRI characteristics of urea-Dex10 and the parent compound Dex10. CEST effects are visualized using so-called Z-spectra in which the reduction of the normalized water signal intensity (S/S_0) is displayed as a function of RF saturation frequency offset (ω) relative to the water protons. The water-proton frequency is set to 0 ppm by convention, and the water signal disappears upon direct saturation at that frequency. The dextran hydroxyl proton saturation transfer to water becomes visible through a slight asymmetry over the 0–2 ppm offset range (Fig. 3a, also see Supplementary Table S1 for the simulated B_0 dependent ω offset to achieve the maximum contrast), which can be better visualized by performing an analysis of the so-called magnetization transfer ratio asymmetry, $MTR_{asym} = (S^{-\omega} - S^{+\omega})/S_0$, with respect to the water signal at 0 ppm (Fig. 3b). The results in this figure show that conjugation to the PSMA-targeting ligand does not appreciably affect the dextran CEST–MRI contrast, which is expected because the particle

contains only 2.5 mmol/mole of free amino group (see Methods). Like Dex10, urea-Dex10 can also be readily detected by CEST–MRI, namely 18 and 20 μM for generating 1% MRI signal change at pH 7.4 and 37°C for Dex10 and urea-Dex10, respectively. As shown in Fig. 3c, d, the pH dependencies are comparable too. These *in vitro* results demonstrate that conjugation with PSMA-targeting ligand has a minimal effect on the CEST signal-detection properties of dextran.

We then injected PSMA-targeted urea-Dex10 in mice bearing isogenic human prostate cancer PSMA(+) PC3-PIP and PSMA(−) PC3-flu tumours, and assessed changes in the dynamic CEST MRI signal in both tumours. This animal model has been validated previously for testing the PSMA-targeting ability of molecular-imaging agents[6,16–18]. As shown in Fig. 4, CEST MRI was able to detect the dynamics of tumour uptake of dextran after urea-Dex10 was administered intravenously at a dose of 375 mg/kg. A substantial increase of > 1% in MTR_{asym} in the mean CEST contrast in both tumour types, that is, 1.28 ± 0.16% and 1.23 ± 0.11% (mean ± s.e.m.) in MTR_{asym} for PC3-PIP and PC3-flu tumours, respectively, could be readily detected at 15 min post-injection (Fig. 4a, b). The increase in CEST contrast was as high as 3% in some regions, presumably within the areas in the vicinity of large tumour vessels (Fig. 4a). After 30 min post-injection, however, there was a decay of CEST contrast in PSMA(−) PC3-flu tumours but not in PSMA(+) PC3-PIP tumours, indicating urea-Dex10 retention in the PSMA(+) tumour due to the presence of PSMA on the tumour cell surface. At 60 min post-injection, the CEST enhancement by urea-Dex10 in the PC3-PIP tumours was more than twice that in the PC3-flu tumours, namely 1.33 ± 0.16% vs. 0.53 ± 0.11% (mean ± s.e.m.) respectively, indicating specificity to PSMA-expressing tumours. That was subsequently confirmed in all mice (n = 5), as shown in the two panels in Fig. 4c, where the CEST signals before and after (60 min) infusion and the difference signals are plotted for both tumour types. To confirm that this higher retention of urea-Dex10 in the PSMA(+) tumours was caused by the specific binding of dextran particles to PSMA, we also injected non-targeted native dextran particles of the same size, Dex10, to another group of animals (see Supplementary Fig. S6 for the CEST plots), showing that the contrast enhancement of Dex10 in PSMA(+) tumours was much weaker than that of urea-Dex10. The bar plots in Fig. 4d show statistically significant differences between the PSMA(+) and PSMA(−) tumours injected with urea-Dex10 (*p* = 0.018, Student's t test, two-tailed and unpaired, n = 5), and between the PSMA(+) tumours injected with urea-Dex10 and non-targeted Dex10 (n = 3, *p* = 0.017, Student's t test, two-tailed and unpaired). Furthermore, pre-treatment of ZJ-43 effectively blocked PSMA and resulted in no observable CEST contrast enhancement in the PSMA(+) tumours (Supplementary Fig. S7). The signal changes of about 1% (or about 1.1 M in water proton concentration) are of the same order of magnitude as functional MRI-signal changes, which are detected routinely with human scanners (> 1.5 T).

In order to validate these *in vivo* MRI results, we also prepared urea-Dex10 conjugated with fluorescence dye (IRDye® 800CW, synthesized according to Fig. S3) for fluorescence imaging and fluorescence microscopy. Although the *in vivo* fluorescence images from the same animal model as the MRI experiments (Fig. 4e) and bio-distribution study using the same fluorescence dye-conjugated urea0Dex10 (Fig. S8) are semi-quantitative, they verify the distinctive fluorescence intensities between the PSMA-expressing tumours vs. those that

to not express PSMA, at 60 min post-injection. Fluorescence-microscopy results (Fig. 4f) also confirmed not only a much higher intensity but also a wider distribution for urea-Dex10 in the PSMA(+) PC3-PIP tumour with respect to the PSMA(−) PC3-flu tumour. Quantitative analysis of the mean fluorescence intensity (Fig. 4g) also showed nearly two times more dextran particles sequestered within the PSMA(+) tumour, in agreement with the MRI findings. These results confirm the specificity of urea-Dex10 to detect PSMA-expressing prostate tumours.

Discussion

PSMA is emerging as the chief biological target for specific imaging of prostate cancer, and is the subject of numerous investigational and clinical studies worldwide using positron emission tomography. Although the urea-based PSMA-targeting ligand forms the basis of a group of emerging clinical radiopharmaceuticals[19], owing to the need for a high concentration of MRI contrast agent, no similar MRI-based methods with potential for clinical translation are available. Our approach employs biocompatible dextran particles on the order of 20 μM, which provide a sufficiently sensitive CEST MRI signal to successfully detect PSMA expression in prostate tumours. The generated MRI contrast was about 1% (or about 1.1 M of water proton concentration), which is of the same order of magnitude as functional-MRI signal changes. The sensitivity of the probe has the potential for rapid clinical translation, as dextrans are currently used clinically for other applications at similar glucose concentrations[20].

CEST contrast by dextran derives from its hydroxyl protons[9,21], which are easily accessible and in rapid exchange with protons of the surrounding water molecules. Similar to glycogen[10], dextran is a branched polysaccharide, and its CEST MRI detectability at a particular size is proportional to its number of glucose units, n. Dextran of higher molecular weight has higher CEST sensitivity on a per-dextran-unit basis, but detectability on a per-glucose-unit basis is similar to those of low-molecular-weight dextrans (Figure S1, see Supplementary Information) and glucose[11,12]. It may at first seem best to use a larger particle for higher per-concentration sensitivity, but it is more difficult for larger particles to penetrate tumours, which could increase the background signal and decrease target-to-background ratio[22].

Our approach has a number of important advantages. First, because it involves clinically compatible agents, it is a safe and translatable MRI-labelling method for receptor-specific imaging. Several types of dextrans are currently used clinically and have a proven safety profile[20]. Similar to all other intravenously administered colloids, dextrans can induce anaphylactoid or anaphylactic reactions through two pathomechanisms: the milder reactions are predominantly anaphylactoid and non–antibody-dependent, and the severe reactions are anaphylactic and only occur in patients with high titers of dextran-reactive antibodies, predominantly immunoglobulin (Ig)G (but not IgE), mast cells and histamine[23,24]. The severe dextran-induced anaphylactoid/anaphylactic reaction can be substantially reduced by dextran 1 (Promit®), making dextran at least as safe as albumin and starches[25,26]. Although we demonstrated receptor binding using dextran as the CEST probe, this approach can be tailored to other clinically available polymers and particles, such as polysaccharides,

polypeptides and proteins. Indeed, sugar polymers are becoming increasingly important for use in the delivery of drugs, including genetic material[27,28], and as molecular tools in cell imaging and in the implementation of vaccines. Second, because the dextran probes don't contain paramagnetic metals, and because clinical-grade dextrans are nonimmunogenic[29], the probes can be potentially used repeatedly without fear of accumulation and toxicity. Third, dextran can be also functionalized to carry drugs such as doxorubicin[30] and methotrexate[31,32], and such theranostic constructs could be used to detect the therapeutic agents. Fourth, dextran is available in a range of particle sizes, enabling the design of CEST MRI probes for specific applications. Overall, the approach may extend receptor- and other protein-targeted imaging to clinical MRI. Although we have developed the dextran probes primarily for improving the diagnosis and treatment of prostate cancer, the approach may also be applied to whole-body screening, as PSMA is also overexpressed in the neovasculature of nearly all non-prostate solid tumors[33]. This will however require the availability of fast CEST sequences (currently under development[34–36]) to keep the clinical exam brief.

Methods

Chemicals and synthetic chemistry

Amino-dextran (MW = 10 kD) was purchased from LifeTechnologies (Grand Island, NY). The material contains 2.5 mmol/mol free amino groups for functionalization. N-hydroxysuccinimide activated ligand (94 mg, 0.2 mmol), which was synthesized from protected Glu and Lys via a 7-step synthesis[37], was dissolved in 10 ml water. To the solution, dextran (compound **1**, Fig. 3) 160 mg (0.016 mmol with 0.04 mmol amino groups) and triethylamine 0.5 mL (excess) were added. The reaction was kept at room temperature for 5 hours. The mixture was loaded to the centrifugal filter units with a cut-off size of 3kD for purification. After washed for five times with 30 mL water, 160 mg of compound **3** was obtained after lyophilization as a white and plastic-like solid. The yield was estimated to be 85 % by the weight of product. The conjugation was confirmed by ^{1}H-NMR spectra (Supplementary Fig. S4.). The mean size (z-average) and size heterogeneity (polydispersity index, PDI) of the synthesized urea-Dex10 was measured in PBS at room temperature by dynamic light scattering (DLS) using a Nanosizer ZS90 (Malvern Instruments, Southborough, MA). The stability of urea-Dex10 at room temperature in PBS was assessed using 1H-NMR for one week.

Receptor binding assay

PSMA inhibitory activities of **1-3** were determined using a fluorescence-based assay according to a previously reported procedure.[17] Briefly, 25 μL lysates of PSMA-positive human prostate adenocarcinoma (LNCaP) cells were incubated with the inhibitor (12.5 μL) in the presence of 4 μM N-acetylaspartylglutamate (NAAG) (12.5 μL) for 120 min. The amount of the glutamate released from NAAG hydrolysis was measured by incubating with a working solution (50 μL) of the Amplex Red Glutamic Acid Kit (Molecular Probes Inc., Eugene, OR) for 60 min. Fluorescence was measured with a VICTOR3V multilabel plate reader (Perkin Elmer Inc., Waltham, MA) with excitation at 530 nm and emission at 560 nm. Inhibition curves were determined using semi-log plots and IC_{50} values were determined at

the concentration at which enzyme activity was inhibited by 50%. Assays were performed in triplicate. Enzyme inhibitory constants (K_i values) were generated using the Cheng-Prusoff conversion.[38] Data analysis was performed using GraphPad Prism version 4.00 for Windows (GraphPad Software, San Diego, California).

Animals

All animal experiments were performed in accordance with protocols approved by our institutional Animal Care and Use Committee. PC3 (human prostate cancer) PIP cells, which have 5×10^6 PSMA receptors per cell, were used to generate the xenografts. Isogenic PSMA- PC3 flu cells were used as a negative control[37]. Both cells were gifts from Dr. Warren Heston (Cleveland Clinic), identified by short tandem repeat analysis, and confirmed no mycoplasma contamination. NOD/SCID mice (6-8 week, male, Charles River Laboratories, Wilmington, MA) were implanted subcutaneously (s.c.) with PSMA(+) PC-3 PIP and PSMA(−) PC-3 flu cells (2×10^6 in 100 μL of Matrigel) at the low right and left flanks, respectively. Mice were imaged when the xenografts reached 5 to 10 mm in diameter. In all the animal experiments, mice were randomly selected for different groups. The investigators were not blinded to the mice in different groups.

MRI studies

The *in vitro* CEST contrast of Dex10 and urea-Dex10 were assessed using a vertical bore Bruker 11.7 T MRI scanner equipped with a 15 mm volume coil, as described previously. [39,40] *In vivo* MR studies were carried out on a Biospec 11.7 T horizontal bore MRI scanner equipped with a 23 mm mouse brain volume coil. CEST MR images were acquired before and within the first hour after the tail vein injection of urea-10 kD-dextran (urea-Dex10) particles at a dose of 375 mg/kg (100 μL of 75 mg/ml saline solution) through the tail vein. For the dynamic study, CEST images were repetitively acquired at the offsets of ±0.6, ±0.8, ±1.0, and ±1.2 ppm. A fat-suppressed RARE sequence with a continuous wave pre-saturation pulse of B1=1.8 μT and 3 seconds (TR/TE=5000/5 ms, RARE factor=10) was used. To correct the B_0 inhomogeneity, two WASSR scans were acquired before and after the CEST acquisitions. Data were processed using custom-written MATLAB scripts. After correcting for B_0 inhomogeneity using the WASSR method,[41] the *in vivo* CEST contrast was quantified by averaging the $MTR_{asym} = (S^{-\omega} - S^{+\omega})/S_0$ at 1.0 ppm. The change in CEST MRI was quantified by $\Delta MTR_{asym}(t) = MTR_{asym}(t) - MTR_{asym}(t0)$.

Fluorescence microscopy

One hour after the injection of fluorescently labelled urea-dextran (IRDye® 800CW-conjugated urea-Dex10, Fig. S5), animals were anesthetized with sodium pentobarbital (50 mg/kg, i.p.), and transcardially perfused with 10 mL 0.9% heparinized saline followed by 10 mL 4% paraformaldehyde in phosphate-buffered saline. After dissection, tumours were post-fixed, cryoprotected with 20% sucrose, frozen in dry ice, and then sliced to 20 μm sections in thickness. Slices were stained with DAPI (Sigma) for the cell nuclei and analyzed using a Zeiss microscope for the co-localization of dextran that were labelled with Li-Cor 800CW dye (ex/em=774/789 nm). The red-fluorescence signal of each image was normalized by the total fluorescence intensity of the corresponding DAPI staining image.

Immunohistochemistry

PSMA(+) PC3 PIP and PSMA(−) PC3 flu tumours from the mice were harvested at 24 h after the MRI studies and fixed in 10% buffered formalin. Tissues were subsequently embedded in paraffin and sectioned at 4 μm thickness. A standard immunohistochemical protocol was performed to stain the tissue sections with anti-PSMA antibody (1:50 dilution, Clone 3E6, Dako, Carpinteria, CA) as described previously[42].

Statistical analysis—The data were expressed as means ± SD and analyzed by the type 2, two-tailed Student's t test where appropriate. Differences were considered significant at $P < 0.05$. Sample sizes were chosen to ensure adequate power (>80%, at significance of 0.05) to detect predicted effect sizes, which were estimated on the basis of either preliminary data or previous experiences with similar experiments. Data followed a normal distribution with similar variance. No exclusion criteria were imposed; therefore all mice were included in analysis.

Data availability—The authors declare that all data supporting the findings of this study are available within the paper and its Supplementary Information. Source data for the figures in this study are available in figshare with the identifier http://dx.doi.org/10.6084/m9.figshare.4981580

Supplementary Material

Refer to Web version on PubMed Central for supplementary material.

Acknowledgments

References

1. Mahajan A, et al. Bench to bedside molecular functional imaging in translational cancer medicine: to image or to imagine? Clin Radiol. 2015; 70:1060–1082. [PubMed: 26187890]

2. Hajdu I, et al. Cancer cell targeting and imaging with biopolymer-based nanodevices. Int J Pharm. 2013; 441:234–241. [PubMed: 23246780]

3. Cohen B, Dafni H, Meir G, Harmelin A, Neeman M. Ferritin as an endogenous MRI reporter for noninvasive imaging of gene expression in C6 glioma tumors. Neoplasia. 2005; 7:109–117. [PubMed: 15802016]

4. Artemov D, Mori N, Ravi R, Bhujwalla ZM. Magnetic resonance molecular imaging of the HER-2/neu receptor. Cancer Res. 2003; 63:2723–2727. [PubMed: 12782573]

5. Tse BW, et al. PSMA-targeting iron oxide magnetic nanoparticles enhance MRI of preclinical prostate cancer. Nanomedicine (Lond). 2015; 10:375–386. [PubMed: 25407827]

6. Banerjee SR, et al. Synthesis and Evaluation of GdIII-Based Magnetic Resonance Contrast Agents for Molecular Imaging of Prostate-Specific Membrane Antigen. Angewandte Chemie International Edition. 2015; 54:10778–10782. [PubMed: 26212031]

7. Pu F, et al. Prostate-specific membrane antigen targeted protein contrast agents for molecular imaging of prostate cancer by MRI. Nanoscale. 2016; 8:12668–12682. [PubMed: 26961235]

8. Holmes EH. PSMA specific antibodies and their diagnostic and therapeutic use. Expert opinion on investigational drugs. 2001; 10:511–519. [PubMed: 11227049]

9. Ward KM, Aletras AH, Balaban RS. A new class of contrast agents for MRI based on proton chemical exchange dependent saturation transfer (CEST). J Magn Reson. 2000; 143:79–87. [PubMed: 10698648]

10. van Zijl PC, Jones CK, Ren J, Malloy CR, Sherry AD. MRI detection of glycogen in vivo by using chemical exchange saturation transfer imaging (glycoCEST). Proc Natl Acad Sci U S A. 2007; 104:4359–4364. [PubMed: 17360529]

11. Chan KW, et al. Natural D-glucose as a biodegradable MRI contrast agent for detecting cancer. Magn Reson Med. 2012; 68:1764–1773. [PubMed: 23074027]

12. Walker-Samuel S, et al. In vivo imaging of glucose uptake and metabolism in tumors. Nat Med. 2013; 19:1067–1072. [PubMed: 23832090]

13. Armstrong JK, Wenby RB, Meiselman HJ, Fisher TC. The hydrodynamic radii of macromolecules and their effect on red blood cell aggregation. Biophys J. 2004; 87:4259–4270. [PubMed: 15361408]

14. Dreher MR, et al. Tumor vascular permeability, accumulation, and penetration of macromolecular drug carriers. J Natl Cancer Inst. 2006; 98:335–344. [PubMed: 16507830]

15. Chen Y, et al. 2-(3-{1-Carboxy-5-[(6-[18F]fluoro-pyridine-3-carbonyl)-amino]-pentyl}-ureido)- pen tanedioic acid, [18F]DCFPyL, a PSMA-based PET imaging agent for prostate cancer. Clin Cancer Res. 2011; 17:7645–7653. [PubMed: 22042970]

16. Chandran SS, Banerjee SR, Mease RC, Pomper MG, Denmeade SR. Characterization of a targeted nanoparticle functionalized with a urea-based inhibitor of prostate-specific membrane antigen (PSMA). Cancer Biol Ther. 2008; 7:974–982. [PubMed: 18698158]

17. Banerjee SR, et al. Sequential SPECT and optical imaging of experimental models of prostate cancer with a dual modality inhibitor of the prostate-specific membrane antigen. Angewandte Chemie International Edition. 2011; 50:9167–9170. [PubMed: 21861274]

18. Ray Banerjee S, et al. Effect of chelators on the pharmacokinetics of (99m)Tc-labeled imaging agents for the prostate-specific membrane antigen (PSMA). Journal of medicinal chemistry. 2013; 56:6108–6121. [PubMed: 23799782]

19. Szabo Z, et al. Initial Evaluation of [(18)F]DCFPyL for Prostate-Specific Membrane Antigen (PSMA)-Targeted PET Imaging of Prostate Cancer. Mol Imaging Biol. 2015; 17:565–574. [PubMed: 25896814]

20. Dubick MA, Wade CE. A review of the efficacy and safety of 7.5% NaCl/6% dextran 70 in experimental animals and in humans. Journal of Trauma-Injury, Infection, and Critical Care. 1994; 36:323–330.

21. Cobb JG, Li K, Xie J, Gochberg DF, Gore JC. Exchange-mediated contrast in CEST and spin-lock imaging. Magn Reson Imaging. 2014; 32:28–40. [PubMed: 24239335]

22. Kobayashi H, Longmire MR, Ogawa M, Choyke PL. Rational chemical design of the next generation of molecular imaging probes based on physics and biology: mixing modalities, colors and signals. Chem Soc Rev. 2011; 40:4626–4648. [PubMed: 21607237]

23. Hedin H, Richter W. Pathomechanisms of dextran-induced anaphylactoid/anaphylactic reactions in man. Int Arch Allergy Appl Immunol. 1982; 68:122–126. [PubMed: 6176555]

24. Kraft D, et al. Immunoglobulin class and subclass distribution of dextran-reactive antibodies in human reactors and non reactors to clinical dextran. Allergy. 1982; 37:481–489. [PubMed: 6185010]

25. Ljungström KG. Dextran 40 therapy made safer by pretreatment with dextran 1. Plastic and reconstructive surgery. 2007; 120:337–340. [PubMed: 17572583]

26. Zinderman CE, Landow L, Wise RP. Anaphylactoid reactions to Dextran 40 and 70: reports to the United States Food and Drug Administration, 1969 to 2004. J Vasc Surg. 2006; 43:1004–1009. [PubMed: 16678697]

27. Eroglu M, Oner E, Mutlu E, Bostan M. Sugar Based Biopolymers in Nanomedicine; New Emerging Era for Cancer Imaging and Therapy. Current topics in medicinal chemistry. 2016

28. Banerjee A, Bandopadhyay R. Use of dextran nanoparticle: A paradigm shift in bacterial exopolysaccharide based biomedical applications. Int J Biol Macromol. 2016; 87:295–301. [PubMed: 26927936]

29. Ljungstrom KG. Dextran 40 therapy made safer by pretreatment with dextran 1. Plast Reconstr Surg. 2007; 120:337–340. [PubMed: 17572583]

30. Danhauserriedl S, et al. Phase-I Clinical and Pharmacokinetic Trial of Dextran Conjugated Doxorubicin (Ad-70, Dox-Oxd). Invest New Drugs. 1993; 11:187–195. [PubMed: 7505268]

31. Varshosaz J. Dextran conjugates in drug delivery. Expert Opin Drug Deliv. 2012; 9:509–523. [PubMed: 22432550]

32. Nevozhay D, et al. Antitumor properties and toxicity of dextran-methotrexate conjugates are dependent on the molecular weight of the carrier. Anticancer Res. 2006; 26:1135–1143. [PubMed: 16619515]

33. Silver DA, Pellicer I, Fair WR, Heston WD, Cordon-Cardo C. Prostate-specific membrane antigen expression in normal and malignant human tissues. Clin Cancer Res. 1997; 3:81–85. [PubMed: 9815541]

34. Zhang Y, et al. Chemical exchange saturation transfer (CEST) imaging with fast variably-accelerated sensitivity encoding (vSENSE). Magn Reson Med. 2017; 77:2225–2238. [PubMed: 27364631]

35. Heo HY, et al. Accelerating chemical exchange saturation transfer (CEST) MRI by combining compressed sensing and sensitivity encoding techniques. Magn Reson Med. 2017; 77:779–786. [PubMed: 26888295]

36. Zhang S, et al. Balanced Steady-State Free Precession (bSSFP) from an effective field perspective: Application to the detection of chemical exchange (bSSFPX). J Magn Reson. 2017; 275:55–67. [PubMed: 28012297]

37. Banerjee SR, et al. A modular strategy to prepare multivalent inhibitors of prostate-specific membrane antigen (PSMA). Oncotarget. 2011; 2:1244–1253. [PubMed: 22207391]

38. Cheng Y, Prusoff WH. Relationship between the inhibition constant (K1) and the concentration of inhibitor which causes 50 per cent inhibition (I50) of an enzymatic reaction. Biochem Pharmacol. 1973; 22:3099–3108. [PubMed: 4202581]

39. Liu G, Gilad AA, Bulte JW, van Zijl PC, McMahon MT. High-throughput screening of chemical exchange saturation transfer MR contrast agents. Contrast Media Mol Imaging. 2010; 5:162–170. [PubMed: 20586030]

40. Li Y, et al. CEST theranostics: label-free MR imaging of anticancer drugs. Oncotarget. 2016; 7:6369–6378. [PubMed: 26837220]

41. Kim M, Gillen J, Landman BA, Zhou J, van Zijl P. Water saturation shift referencing (WASSR) for chemical exchange saturation transfer (CEST) experiments. Magnetic Resonance in Medicine. 2009; 61:1441–1450. [PubMed: 19358232]

42. Chen Y, et al. A PSMA-targeted theranostic agent for photodynamic therapy. J Photochem Photobiol B. 2017; 167:111–116. [PubMed: 28063300]
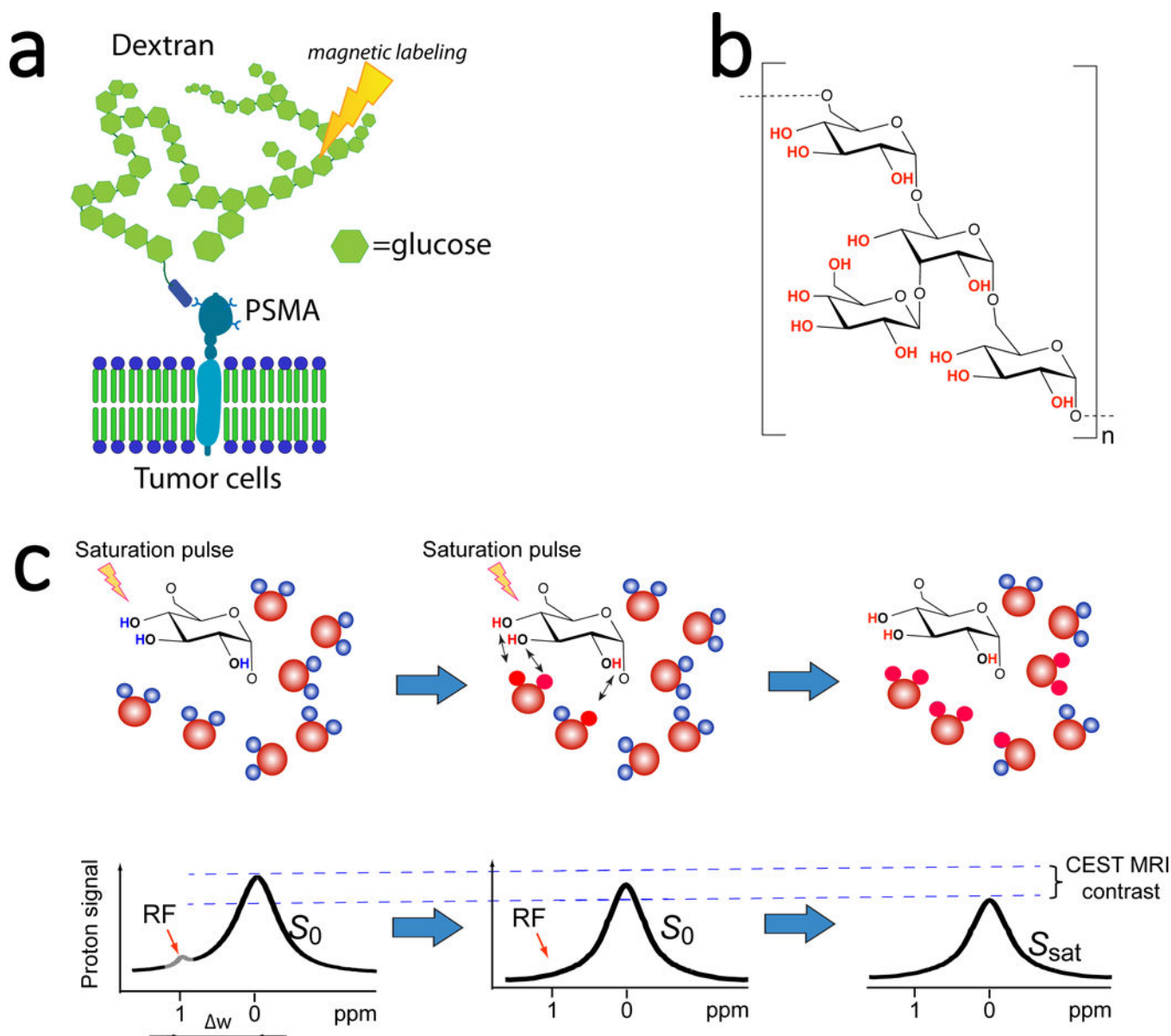
Figure 1. Development of dextran-based contrast agents for PSMA-receptor MR imaging
a) Illustration of PSMA targeting and MRI detection of dextran-based agents that uses only RF-based magnetic labelling (signal saturation) without the need for metallic or radioactive labels. **b**) The chemical composition of dextran. **c**) Illustration of CEST MRI detection of natural dextran, which is achieved by the continuous transfer of saturated protons (red) from hydroxyl groups to surrounding water molecules, generating a reduction in the water signal (MRI contrast) proportional to the dextran concentration and rate of exchange.
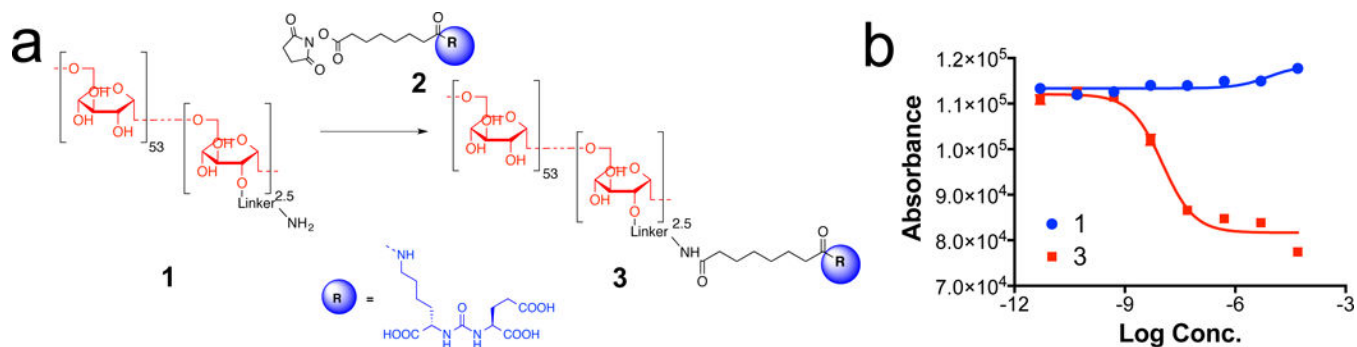
Figure 2. Synthesis and characterization of PSMA-targeting dextran

a) Synthetic scheme of PSMA targeting Dex10 urea-Dex10 (compound **3**); b) PSMA receptor binding abilities of Dex10 (compound **1**) and urea-Dex10 (compound **3**) from a fluorescence-based assay for the inhibition on the hydrolysis of *N*-acetylaspartylglutamate (NAAG) to glutamate by the lysates of PSMA-positive human prostate adenocarcinoma (LNCaP) cells for 2 hours. K_i = 2 nM for urea-Dex 10.
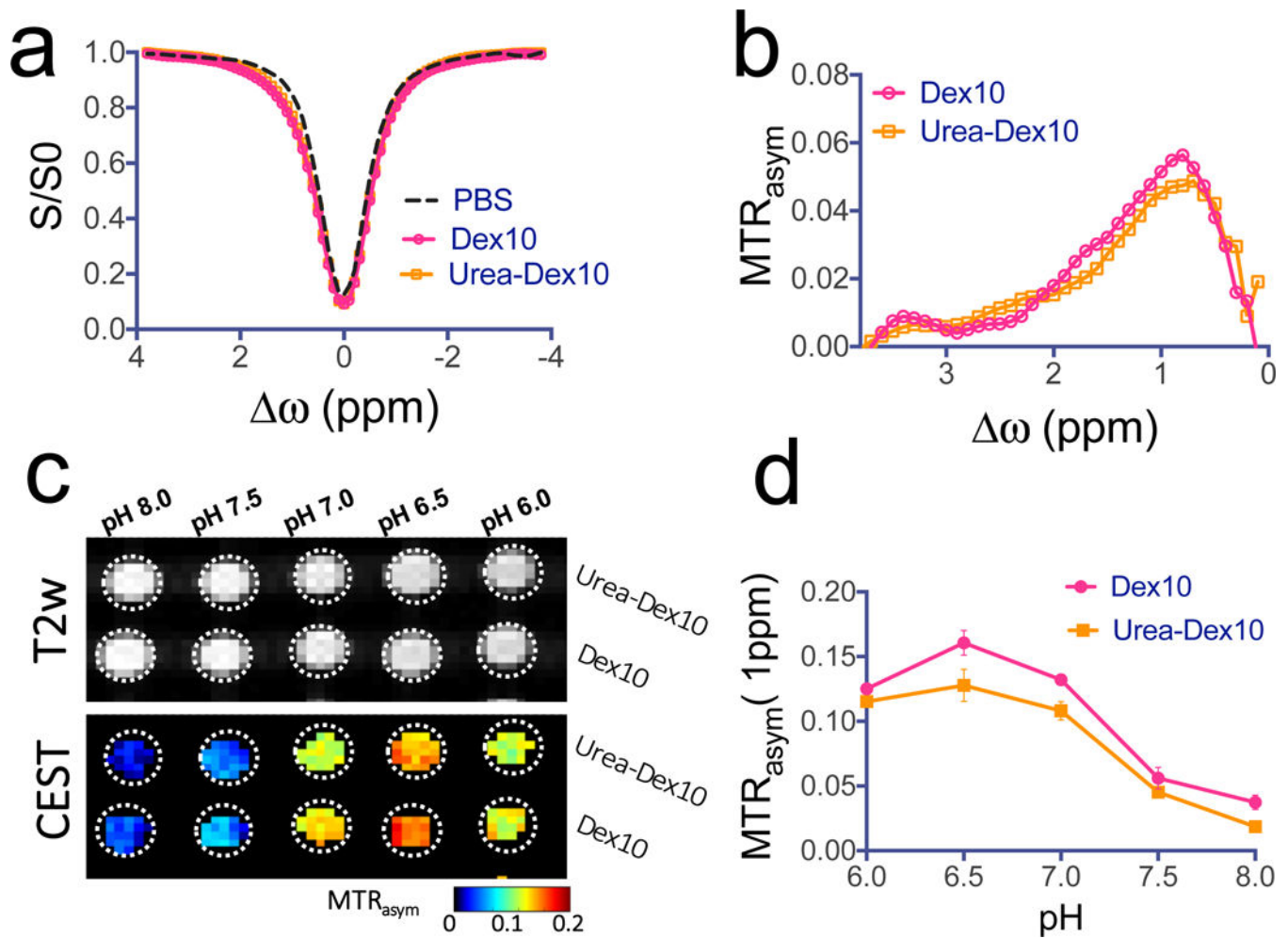
Figure 3. CEST MRI detection of dextrans

a) Z-spectra and **b**) MTR_asym plots showing the CEST effects of PSMA-targeted urea-Dex10 and non-targeted Dex10 at 1 mg/mL, pH 7.4 and 37°C. **c**) T2-weighted and CEST (MTR_asym) images of 1 mg/mL urea-Dex10 and 1 mg/mL Dex10 at different pH values. **d**) Comparison of the pH dependence of the CEST signal at 1 ppm of urea-Dex10 and Dex10 at 1 mg/mL, pH 7.4 and 37°C, indicating the functionalization of Dex10 does not alter CEST effects. All measurements were acquired using a rectangular RF pulse with strength B1 = 4.7 µT and length t_{sat} = 3 seconds. Molar concentrations of 1 mg/mL correspond to approximately 90 and 100 µM of urea-Dex10 and Dex10, respectively. Error bars are the standard deviations of three separate measures.
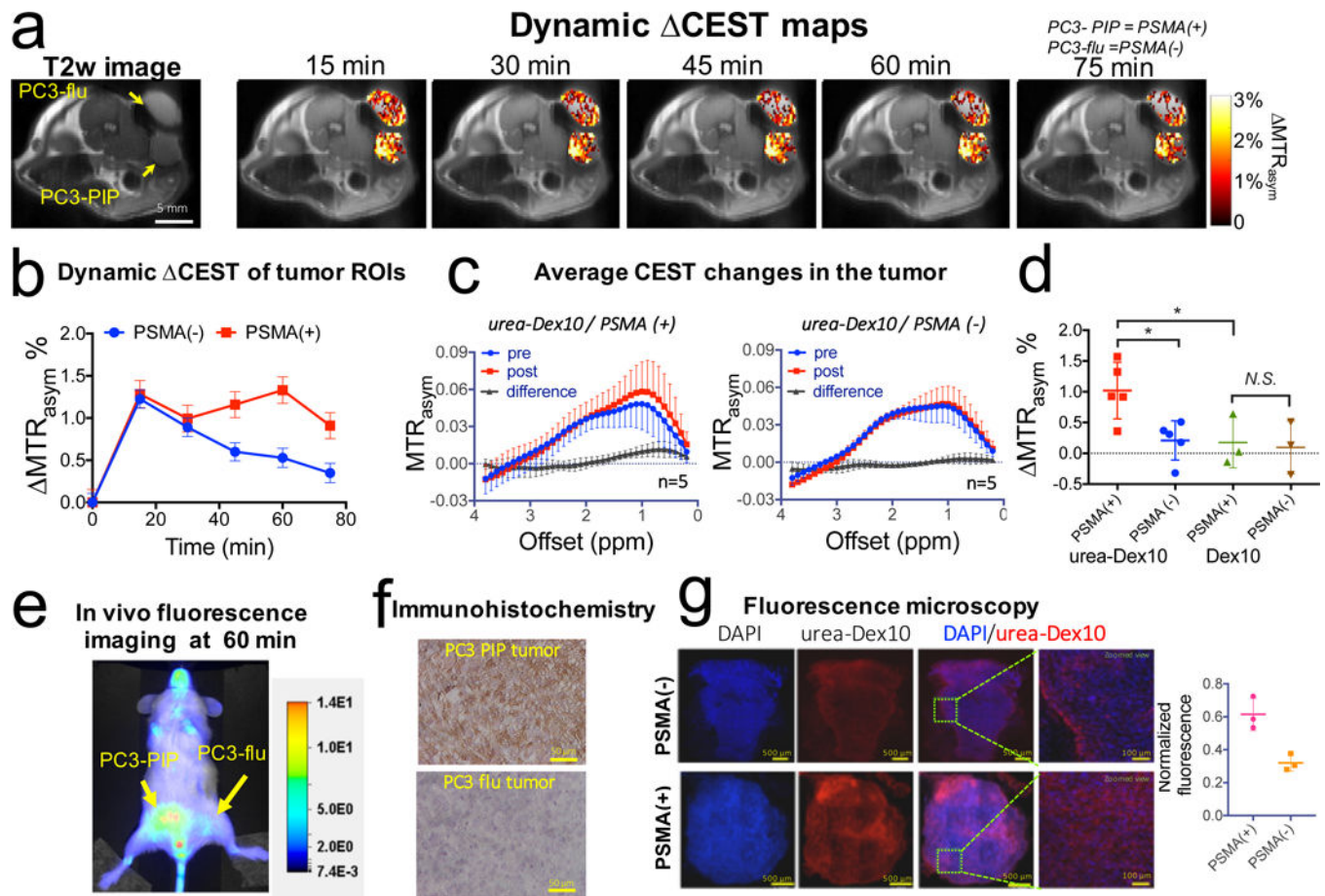
Figure 4. Changes in the dynamic CEST signal in PSMA(+) and PSMA(−) tumours

a) T2-weighted image and dynamic CEST maps at 1 ppm after the injection of 375 mg/kg urea-10KD-dextran (injection volume =100 μL). **b**) Mean changes in the CEST signal in PSMA(+) and PSMA(−) tumours in one of the mice for which time dependence was measured. CEST signal enhancement was quantified by $MTR_{asym} = MTR_{asym}(t)-MTR_{asym}(t=0)$, where the error bars are the standard errors of the CEST signal of all the pixels in each tumour. All CEST images were acquired using a 1.8 μT and 3-second-long CW pulse. **c**) Average CEST signal in the tumour for five mice before (blue) and one hour after (red) the injection of urea-Dex10. The signal difference is shown in black. Error bars are standard deviations of the CEST signal of all five tumours. **d**) Bar plots showing the mean changes in CEST signal as quantified by MTR_{asym} (1 h) in each type tumour (n = 5 and 3 for urea-Dex10 and non-targeted Dex10 respectively). * : $P<0.05$ (Student's t test, two-tailed and unpaired). **e**) In vivo fluorescence image of a representative mouse showing a distinctive tumour uptake of urea-Dex10 at 60 minutes after injection. **f**) Sections of PSMA(+) PC3-PIP (top) and PSMA(−) PC3-flu (bottom) tumours stained with anti-PSMA. Images were acquired at 40× magnification. **g**) Fluorescence microscopy of nuclei (blue, stained with DAPI) dextran (red, NIR-600-labeled). Scale bar= 500 μm for the left three panels and 100 μm for the most right panels, which are the zoomed view of area enclosed in dashed green box in the image on the left. On the right, a scatter plot shows the comparison

of the normalized mean fluorescence intensity of three different field of views in the tumours.